



# K63-linked polyubiquitination of LGP2 by Riplet regulates RIG-I-dependent innate immune response

Takahisa Kouwaki<sup>1</sup>, Tasuku Nishimura<sup>1</sup>, Guanming Wang<sup>1</sup>, Reiko Nakagawa<sup>2</sup>  & Hiroyuki Oshiumi<sup>1,\*</sup> 

## Abstract

Type I interferons (IFNs) exhibit strong antiviral activity and induce the expression of antiviral proteins. Since excessive expression of type I IFNs is harmful to the host, their expression should be turned off at the appropriate time. In this study, we find that post-translational modification of LGP2, a member of the RIG-I-like receptor family, modulates antiviral innate immune responses. The LGP2 protein undergoes K63-linked polyubiquitination in response to cytoplasmic double-stranded RNAs or viral infection. Our mass spectrometry analysis reveals the K residues ubiquitinated by the Riplet ubiquitin ligase. LGP2 ubiquitination occurs with a delay compared to RIG-I ubiquitination. Interestingly, ubiquitination-defective LGP2 mutations increase the expression of type I IFN at a late phase, whereas the mutant proteins attenuate other antiviral proteins, such as SP100, PML, and ANKRD1. Our data indicate that delayed polyubiquitination of LGP2 fine-tunes RIG-I-dependent antiviral innate immune responses at a late phase of viral infection.

**Keywords** innate immunity; LGP2; ubiquitination; virus

**Subject Categories** Microbiology, Virology & Host Pathogen Interaction; Post-translational Modifications & Proteolysis

**DOI** 10.15252/embr.202254844 | Received 12 February 2022 | Revised 17 November 2022 | Accepted 28 November 2022 | Published online 14 December 2022

**EMBO Reports (2023) 24: e54844**

## Introduction

RIG-I-like receptors (RLRs) are cytoplasmic viral RNA sensors that trigger antiviral innate immune responses. This includes type I interferon (IFN) production that induces the expression of antiviral proteins (Hur, 2019; Onomoto *et al*, 2021). Recent studies have revealed crucial roles of RLRs in antiviral innate immune response against SARS-CoV-2 (Liu *et al*, 2021; Wu *et al*, 2021; Yamada *et al*, 2021). However, prolonged expression of type I IFNs is

harmful to the host, and hypermorphic mutations in the genes that encode RLRs have been reported to cause autoimmune diseases (Jang *et al*, 2015; Makela *et al*, 2015). Thus, type I IFN and IFN-induced antiviral states should be regulated appropriately.

RLRs consist of three members, RIG-I, MDA5, and LGP2. RIG-I recognizes 5'-triphosphated short double-stranded RNAs (dsRNAs), whereas MDA5 recognizes longer dsRNAs, over 1 Kbp (Kato *et al*, 2008; Onomoto *et al*, 2021). After recognizing viral RNAs, RIG-I and MDA5 bind to the MAVS adaptor molecule through their N-terminal caspase activation and recruitment domains (CARDs), which results in type I IFN expression (Kawai *et al*, 2005; Meylan *et al*, 2005; Seth *et al*, 2005; Xu *et al*, 2005). Although the other member, the LGP2 protein, binds to viral RNAs, the protein lacks an N-terminal CARD domain, and thus cannot induce type I IFN expression alone (Yoneyama *et al*, 2005). Previous studies have reported that LGP2 plays a regulatory role in RLR-mediated type I IFN expression (Venkataraman *et al*, 2007; Satoh *et al*, 2010).

The C-terminal domain (CTD) of the RIG-I protein suppresses its N-terminal CARDs in the absence of viral RNAs, and this suppression is released after the CTD binds to viral RNAs (Saito *et al*, 2007). The CTD of LGP2, which is similar to that of RIG-I, also has a suppressive effect, and it has been reported that LGP2 is a negative regulator of RIG-I (Yoneyama *et al*, 2005; Saito *et al*, 2007). Studies have shown that LGP2 attenuates the RIG-I-mediated innate immune responses after viral infection (Saito *et al*, 2007; Venkataraman *et al*, 2007; Si-Tahar *et al*, 2014). In contrast, there are several reports indicating that LGP2 plays a positive role in the antiviral response, and augments RIG-I- and MDA5-dependent innate immune responses (Satoh *et al*, 2010). The mechanisms underlying the apparent discrepancy remain unclear.

The Riplet protein is an E3 ubiquitin ligase (Oshiumi *et al*, 2013; Cadena *et al*, 2019). Riplet binds to the helicase and the CTD of RIG-I and mediates K63-linked polyubiquitination of the RIG-I protein (Oshiumi *et al*, 2009, 2013). TRIM25 and other E3 ubiquitin ligases have been reported to ubiquitinate the RIG-I protein *in vitro* and/or *in vivo* (Gack *et al*, 2007; Kuniyoshi *et al*, 2014; Yan *et al*, 2014). Post-translational modifications are essential regulatory

<sup>1</sup> Department of Immunology, Graduate School of Medical Sciences, Faculty of Life Sciences, Kumamoto University, Kumamoto, Japan

<sup>2</sup> Laboratory for Phyloinformatics, RIKEN Center for Biosystems Dynamics Research in Kobe, Kobe, Japan

\*Corresponding author. Tel: +81 96 373 5135; E-mail: oshiumi@kumamoto-u.ac.jp

mechanisms of the activities of RLRs (Chiang & Gack, 2017). Indeed, SARS-CoV-2 inhibits ISGylation of MDA5, thereby escaping from host innate immune responses (Liu et al, 2021). Knockout of Riplet markedly reduces the expression of type I IFNs and other pro-inflammatory cytokines following viral infection, such as vesicular stomatitis virus, Sendai virus, and influenza A virus, which are primarily recognized by RIG-I (Oshiumi et al, 2010; Cadena

et al, 2019). Recently, Hur and colleagues have reported that the LGP2 binds to TRIM14, a member of TRIM family including E3 ubiquitin ligases (Kato et al, 2021); however, physiological significance of LGP2 ubiquitination remains unclear. In the present study, we observed K63-linked polyubiquitination of LGP2 by Riplet at a late phase after viral infection. Polyubiquitination of LGP2 attenuated RIG-I-dependent type I IFN expression, but markedly increased the

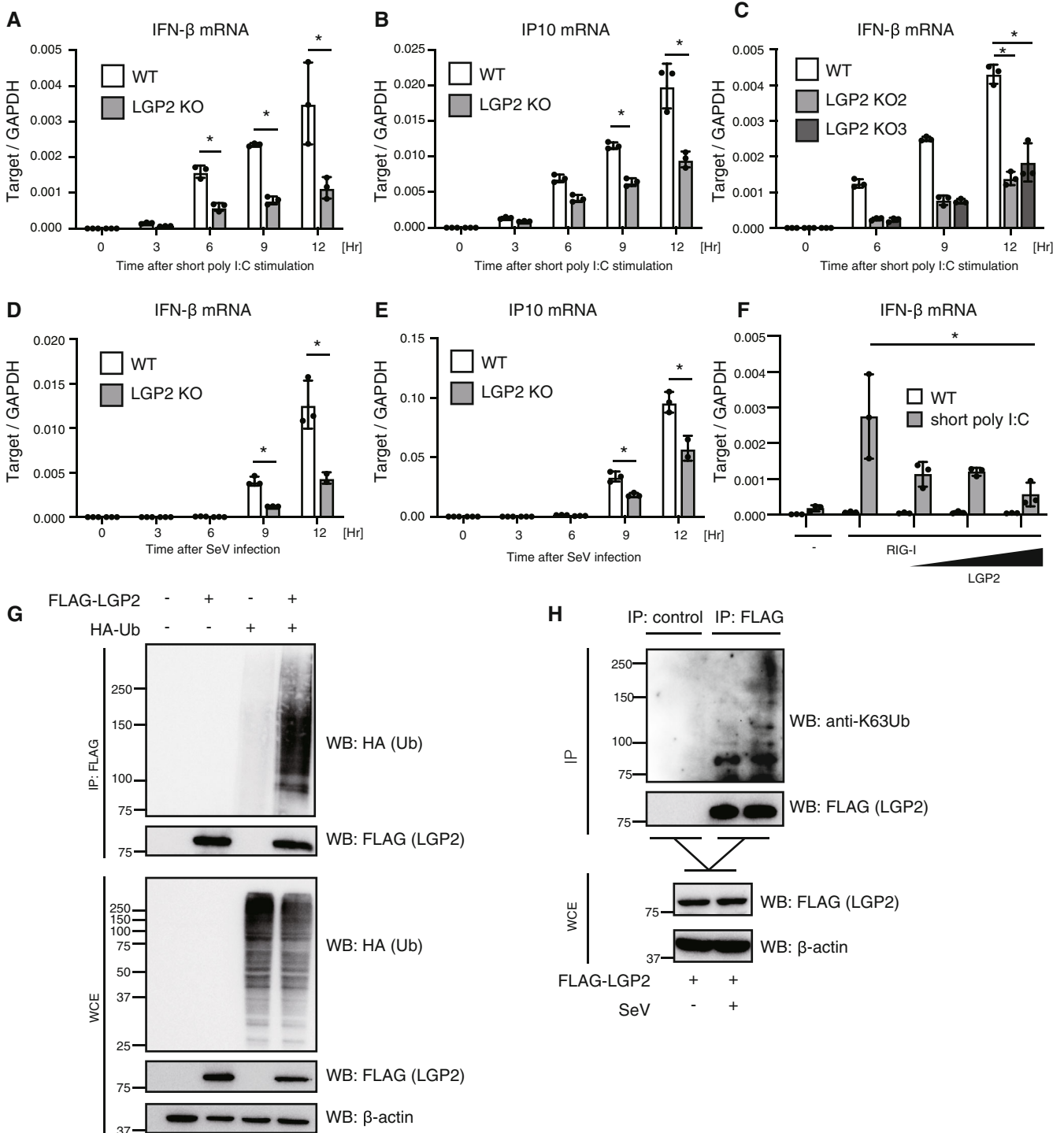


Figure 1.

**Figure 1. Polyubiquitination of LGP2.**

- A–E Wild-type and LGP2-KO HEK293 cells in 24-well plates were transfected with 200 ng/ml of short poly I:C or infected with SeV. IFN- $\beta$  and IP-10 mRNA expression was determined by RT-qPCR. The data represent the mean  $\pm$  SD ( $n = 3$ , t-test,  $*P < 0.05$ ). LGP2 KO2 and KO3 are independently isolated LGP2 KO clones.
- F HEK293 cells in 24-well plates were transfected with LGP2 (0.1, 0.3, or 0.6  $\mu$ g/well) and RIG-I (0.1  $\mu$ g/well) expression vectors as indicated. Twenty-four hours after transfection, cells were stimulated with 200 ng of short poly I:C for 4 h. Total RNAs were extracted, and the expression of IFN- $\beta$  mRNA was determined by RT-qPCR and normalized to GAPDH ( $n = 3$ , t-test,  $*P < 0.05$ ).
- G HEK293FT cells were transfected with FLAG-tagged LGP2 and HA-tagged ubiquitin expression vectors. Whole cell extracts (WCE) were prepared 24 h after transfection. Immunoprecipitation was performed with anti-FLAG antibody (IP: FLAG) and the proteins were detected by western blot analysis with the indicated antibodies.
- H FLAG-tagged LGP2 was transfected into HEK293 cells. Cells were then infected with SeV at MOI = 10 for 24 h. Immunoprecipitation was performed with anti-FLAG antibody, and the proteins were detected with the indicated antibodies.

Data information: All data are representative of at least two independent experiments, and “ $n$ ” represents the number of samples (biological replicates). Error bars represent standard deviation from the mean.

Source data are available online for this figure.

expression of several other antiviral genes including PML and SP100 (Gongora *et al*, 1997; Nguyen *et al*, 2001). Our findings identify a mechanism of a transition of the expression patterns of antiviral genes after viral infection.

## Results

### Dual roles of LGP2 in RIG-I signaling

Previous studies reported positive and negative effects of LGP2 on RIG-I-mediated cytokine expression (Venkataraman *et al*, 2007; Satoh *et al*, 2010). To determine the role of LGP2 in RIG-I signaling under similar experimental conditions, we used HEK293 cells, which are frequently used for RIG-I functional studies. LGP2 knockout (KO) cells were generated using CRISPR-Cas9 system, and we confirmed that the isolated LGP2 KO clones had frameshift mutations in the *lgp2* gene (Fig EV1A and B). WT and LGP2 KO HEK293 cells were transfected with short poly I:C, a ligand of RIG-I, and cytokine expression was measured by RT-qPCR. LGP2 knockout reduced the expression of IFN- $\beta$  and IP-10 mRNA moderately after a short poly I:C stimulation, indicating a positive role for LGP2 in RIG-I signaling under these experimental conditions (Fig 1A and B). Other LGP2 KO clones (KO2 and 3) also exhibited a defect in the cytokine expression in response to the RIG-I ligand (Fig 1C). Sendai virus (SeV) is primarily recognized by RIG-I (Kato *et al*, 2006), and SeV-induced expression of IFN- $\beta$  and IP-10 mRNA was also reduced by LGP2 knockout (Fig 1D and E). Although high ectopic expression of LGP2 moderately reduced RIG-I protein levels by unknown reason, low ectopic expression of LGP2 reduced RIG-I-mediated IFN- $\beta$  promoter activity without reduction of the RIG-I protein levels (Fig EV1C). In addition, overexpression of LGP2 reduced IFN- $\beta$  mRNA expression in response to short poly I:C stimulation (Fig 1F), which is consistent with previous studies that indicated LGP2 as a negative regulator (Yoneyama *et al*, 2005; Venkataraman *et al*, 2007; Si-Tahar *et al*, 2014). These data suggest that LGP2 has both positive and negative roles in RIG-I signaling, at least under our experimental conditions.

### Polyubiquitination of LGP2

There are several possibilities underlying the contradictory phenotypes. One possible explanation is that post-translational modifications may switch between positive and negative functions of LGP2. Since polyubiquitin modifications regulate the RIG-I and MDA5

activities (Davis & Gack, 2015; Chiang & Gack, 2017), we determined whether LGP2 is ubiquitinated. As expected, our immunoprecipitation assay showed that HA-tagged ubiquitin (HA-Ub) were efficiently incorporated into over-expressed LGP2 even in the absence of stimulation (Fig 1G). Next, we used an anti-K63-linked polyubiquitin chain (K63-Ub) antibody to detect ubiquitinated LGP2. Interestingly, exogenously expressed LGP2 underwent K63-linked polyubiquitination in response to SeV infection (Fig 1H).

Since RIG-I undergoes ubiquitination, we compared ubiquitination kinetics of LGP2 with that of RIG-I. Interestingly, we found that K63-linked polyubiquitination of RIG-I increased at 6 h after SeV infection, whereas LGP2 polyubiquitination increased at later time points (Fig 2A). Our data suggest that LGP2 polyubiquitination is delayed compared with RIG-I polyubiquitination. The proximity ligation assay (PLA) can detect close associations between two proteins within cells (Fredriksson *et al*, 2002; Soderberg *et al*, 2006). If LGP2 is polyubiquitinated, it is expected that the PLA signals of LGP2 and ubiquitin are detectable. The HA-Ub expressing vector was transfected into A549 cells, and PLA was performed with anti-HA, anti-RIG-I, and anti-LGP2 antibodies. The PLA signals for RIG-I/HA-Ub and LGP2/HA-Ub were detected, and the number of the PLA signals was increased after short poly I:C stimulation (Fig 2B). Next, we used anti-K63-Ub antibody. HEK293 cells were transfected with LGP2 and the PLA was performed with anti-LGP2 and anti-K63-Ub antibodies. A significant number of PLA signals were detected in LGP2-transfected cells (Fig 2C). When cells were stimulated with rhodamine-conjugated short poly I:C, several PLA signals for LGP2/K63-Ub were co-localized with short poly I:C (Fig EV1D). These data are consistent with our observation that LGP2 was polyubiquitinated. Next, we compared the kinetics of the PLA signals of anti-RIG-I and anti-K63-Ub antibodies (RIG-I/K63-Ub) with that of anti-LGP2 and anti-K63-Ub antibodies (LGP2/K63-Ub). The PLA signals for RIG-I/K63-Ub and LGP2/K63-Ub appeared after a short poly I:C stimulation, and the kinetics of LGP2/K63-Ub were delayed compared with that of RIG-I/K63-Ub (Fig 2D–F). These data are consistent with the observation that polyubiquitination of LGP2 was delayed compared with RIG-I ubiquitination (Fig 2A).

### Riplet mediates the ubiquitination of LGP2

Next, we investigated whether Riplet E3 ubiquitin ligase is involved in the ubiquitination of LGP2, because structural similarity has been reported between the CTDs of LGP2 and RIG-I (Cui *et al*, 2008). First, we investigated whether Riplet binds to LGP2 as to RIG-I. HA-tagged Riplet was co-immunoprecipitated with FLAG-tagged LGP2

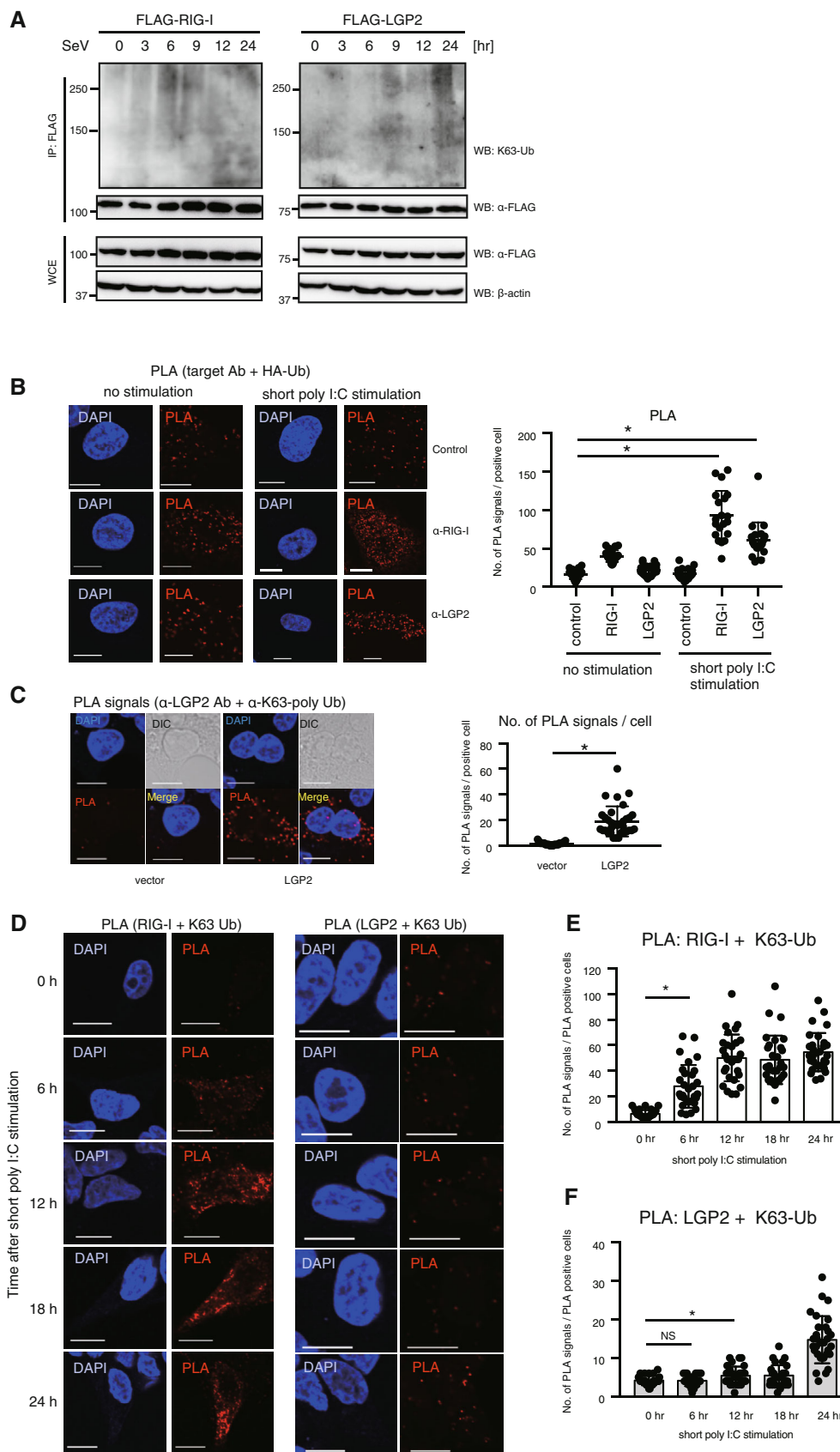


Figure 2.

**Figure 2. Kinetics of LGP2 ubiquitination.**

- A HEK293 cells were transfected with FLAG-RIG-I or FLAG-LGP2 expressing vector. Cells were then infected with SeV, and whole cell extracts were collected at indicated time points. Immunoprecipitation was performed with anti-FLAG antibody. The proteins were subjected to SDS-PAGE and detected by western blotting.
- B A549 cells transfected with HA-tagged ubiquitin were stimulated with 200 ng/ml of short poly I:C for 6 h. PLA was performed with anti-HA, anti-RIG-I, and anti-LGP2 antibodies. The number of PLA signals were counted (*t*-test, \**P* < 0.05, *n* = 20).
- C HEK293 cells were transfected with empty and LGP2 expression vectors for 24 h. PLA was performed with anti-LGP2 and anti-K63-Ub antibodies. The number of PLA signals were counted (*t*-test, \**P* < 0.05, *n* = 33).
- D–F HEK293 cells were transfected with 200 ng/ml of short poly I:C. Cells were fixed at the indicated time points, and PLA was performed with anti-RIG-I, anti-LGP2, and anti-K63-Ub antibodies (D). The number of PLA signals were counted (E, F) (*t*-test, \**P* < 0.05, *n* = 30). Each dot represents the number of PLA signals of each cell.

Data information: Scale bars represent 10  $\mu$ m. All data are representative of at least two independent experiments, and “*n*” represents the number of samples (biological replicates). Error bars represent standard deviation from the mean.

Source data are available online for this figure.

(Fig 3A) and endogenous Riplet protein was also co-immunoprecipitated with FLAG-tagged LGP2 (Fig 3B), suggesting that Riplet binds to LGP2. Interestingly, HA-Ub was efficiently incorporated into LGP2 by Riplet overexpression (Fig 3C). Myc-tagged mutant ubiquitin, K63-only Ub, in which all K residues except K63 are replaced with R, was also efficiently incorporated into LGP2 by Riplet overexpression (Fig 3D). Conversely, knockout of Riplet markedly reduced K63-only Ub incorporation into LGP2 (Fig 3E). Moreover, an increase in the number of the PLA signals of LGP2/K63-Ub was abrogated by knocking out Riplet (Fig 3F and G). These data are consistent with our hypothesis that Riplet mediates K63-linked polyubiquitination of LGP2.

To further test our hypothesis, we performed a mass spectrometry analysis to detect the polyubiquitination of LGP2 by Riplet. A piece of gel containing LGP2 bands that were derived from FLAG-tagged LGP2 and Riplet overexpressing cells was excised and subjected to mass spectrometry analysis (Fig EV2A). We detected several ubiquitin-conjugated LGP2 peptides from FLAG-tagged LGP2 and Riplet overexpressing cells (Fig 4A). The results indicated that K39, K532, K599, and K629 of LGP2 were ubiquitinated (Fig 4A). When RIG-I and LGP2 sequences were aligned, the positions of K532 and K599 of LGP2 were similar to those of K788 and K851 of RIG-I (Fig EV2B). We quantified ubiquitination of the K residues of LGP2 in WT and Riplet-overexpressing cells by analyzing the mass spectrometry data using label-free quantification (LFQ) method. Interestingly, Riplet overexpression increased LFQ values of ubiquitinated K39, K532, and K629, but not K599 (Fig 4A right panels), suggesting that ubiquitination of K39, K532, and K629 were induced

by Riplet overexpression. Since ubiquitination of K599 was not affected by Riplet overexpression (Fig 4A), we do not exclude the possibility that K599 of LGP2 is ubiquitinated by other ubiquitin ligases as well as Riplet. Overall, these data indicate that Riplet mediates the K63-linked polyubiquitination of LGP2.

Previous studies showed that Riplet bound to the CTD and helicase domain of RIG-I. We found that Riplet was co-immunoprecipitated with the CTD and helicase domain of LGP2 (Fig 4B). We constructed a LGP2-4KR mutant, in which the four K residues were replaced with R residues. This was done because E3 ubiquitin ligases cannot ubiquitinate R residues. The 4KR mutations reduced K63-linked polyubiquitination of the LGP2 protein (Fig 4C); however, there were residual polyubiquitinated bands of LGP2-4KR (Fig 4C). These data suggest that not only the four K residues, but also other K residues of LGP2 contain a polyubiquitin chain.

**Polyubiquitination of LGP2 modulates the expression of antiviral genes**

To assess the role of polyubiquitination on the four K residues of LGP2, we constructed LGP2 mutants, in which each K residue was replaced with an R residue. We found that K39R, K532R, and K599R amino acid substitutions in LGP2 exhibited an increased trend of RIG-I-induced IFN- $\beta$  promoter activities, whereas K629R significantly increased the promoter activity (Fig 5A). Additionally, the 4KR mutation also increased the IFN- $\beta$  promoter activity induced by RIG-I (Fig EV3A). Since overexpression of LGP2 from expression vectors exhibited inhibitory effects on RIG-I signaling as shown in

**Figure 3. Riplet mediates K63-linked polyubiquitination of LGP2.**

- A HEK293FT cells were transfected with FLAG-tagged LGP2 and HA-tagged Riplet expression vectors. Twenty-four hours after transfection, cells were lysed, and WCE were prepared. Immunoprecipitation was performed with anti-FLAG antibody, and the proteins were detected by western blotting with the indicated antibodies.
- B HEK293FT cells were transfected with FLAG-tagged LGP2 expression vector. Twenty-four hours after transfection, immunoprecipitation was performed with anti-FLAG antibody and control IgG. Immunoprecipitates were subjected to SDS-PAGE, and the proteins were detected by western blotting with indicated antibodies.
- C HEK293FT cells were transfected with FLAG-tagged LGP2, Riplet, and HA-tagged ubiquitin expression vectors, and immunoprecipitation was performed with anti-FLAG antibody.
- D HEK293FT cells were transfected with FLAG-tagged LGP2, Riplet, and myc-tagged K63-only-Ub expression vectors. Twenty-four hours after transfection, immunoprecipitation was performed with anti-FLAG antibody.
- E WT and Riplet KO HEK293 cells were transfected with FLAG-tagged LGP2 and myc-tagged K63-only-Ub expression vectors, and immunoprecipitation was performed with anti-FLAG antibody.
- F, G WT and Riplet KO HEK293 cells were transfected with 200 ng/ml of short poly I:C for 6 h, and PLA was performed with anti-LGP2 and anti-K63-Ub antibodies. The number of PLA signals were counted (*t*-test, \**P* < 0.05, *n* = 100). Each dot represents the number of PLA signals in each cell. Scale bars represent 10  $\mu$ m.

Data information: All data are representative of at least two independent experiments, and “*n*” represents the number of samples (biological replicates). Error bars represent standard deviation from the mean.

Source data are available online for this figure.

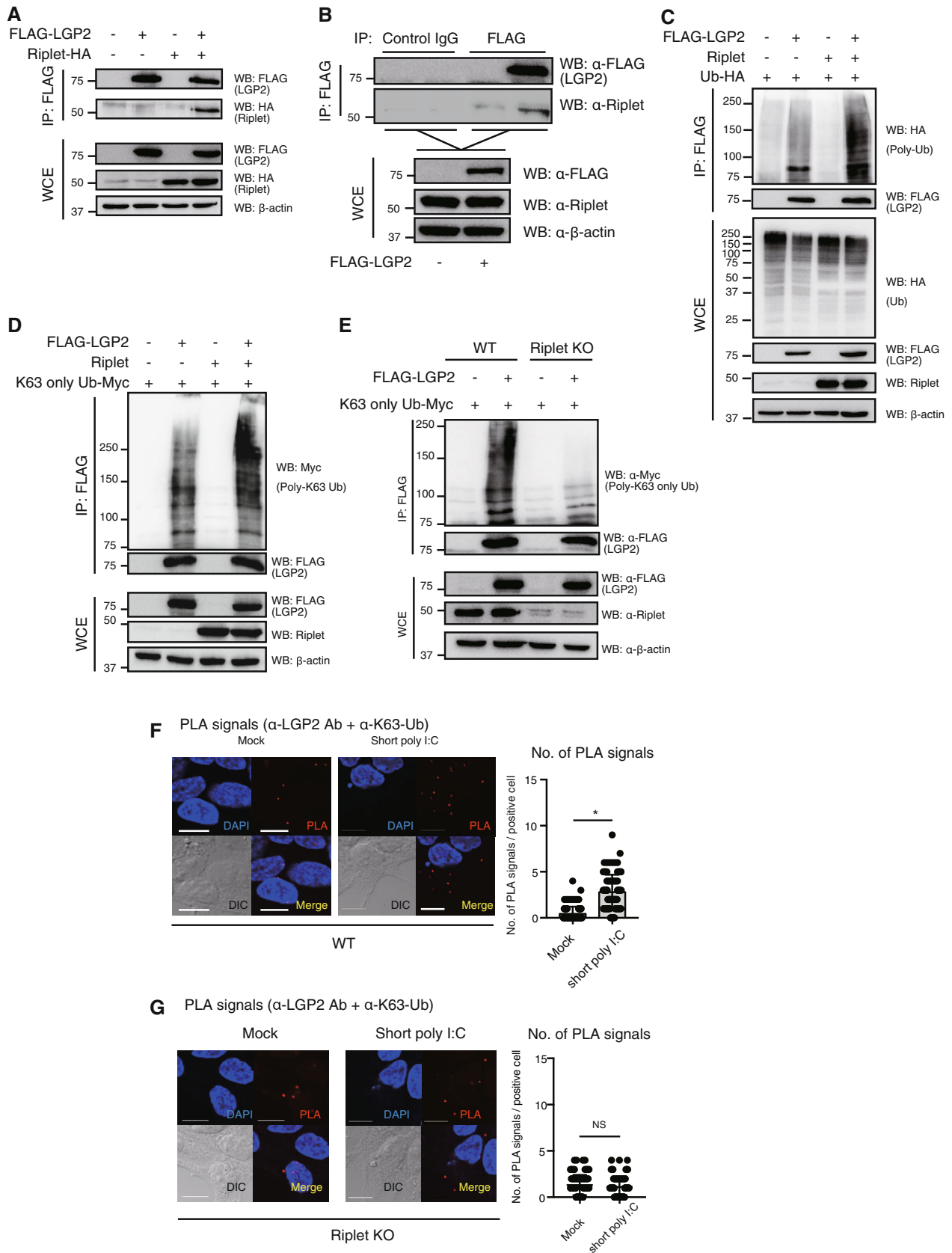


Figure 3.

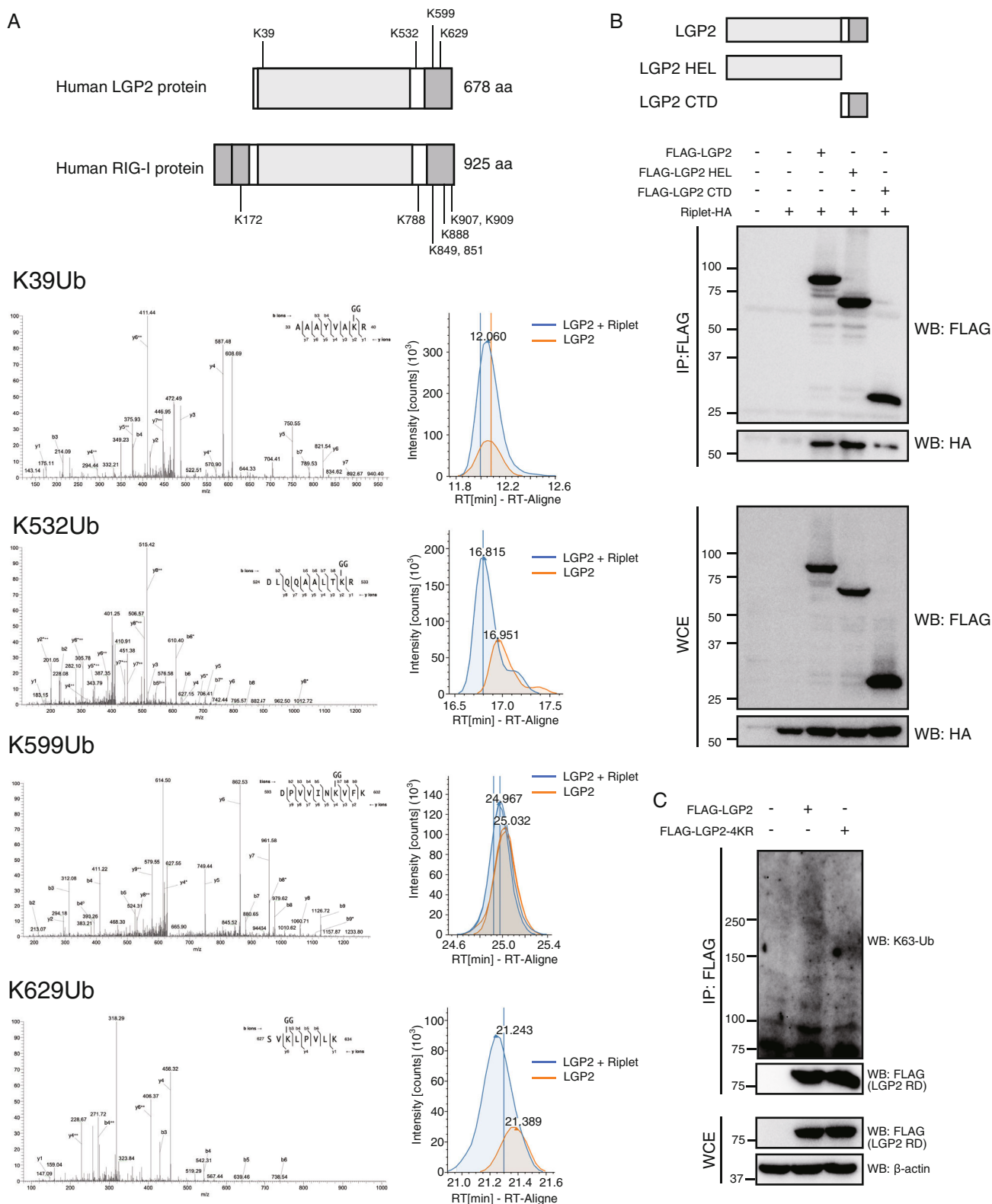


Figure 4.

Fig 1, we generated LGP2-4KR stably expressing HEK293 cells and wild-type LGP2 or GFP (control) stably expressing HEK293 cells. We confirmed that LGP2 expression itself did not attenuate RIG-I

signaling in this condition (Fig 5B). Interestingly, LGP2-4KR expression markedly increased IFN- $\beta$  promoter activity after short poly I:C stimulation (Fig 5B). The expression of IFN- $\beta$ , IP-10, and Ccl5 was

**Figure 4. Ubiquitination sites of LGP2.**

- A Liquid chromatography–tandem mass spectrometry (LC–MS/MS) of LGP2 in Riplet-expressing cells. LC–MS/MS data was quantified using LFQ method. The chromatographic profiles for each ubiquitination site are shown in the right panels. Schematic representation of ubiquitination sites of RIG-I and LGP2 are shown in the upper panel.
- B FLAG-tagged LGP2 fragments and HA-tagged Riplet expression vectors were transfected into HEK293FT cells. Twenty-four hours after transfection WCE were prepared. Immunoprecipitation was performed with anti-FLAG antibody. Immunoprecipitates were subjected to SDS–PAGE, and the proteins were detected by western blotting with indicated antibodies. The data is a representative of two independent experiments.
- C FLAG-tagged LGP2 and FLAG-tagged LGP2-4KR expression vectors were transfected into HEK293FT cells. Twenty-four hours after transfection, WCE were prepared. Immunoprecipitation was performed with anti-FLAG antibody. The data are representative of two independent experiments.

Source data are available online for this figure.

enhanced by LGP2-4KR expression only at late time points after short poly I:C stimulation, SeV infection, or Flu infection (Fig 5C–J). Delayed enhancement of the cytokine expression appeared to be concomitant with delayed ubiquitination of LGP2 (Fig 2A). To further assess the role of the 4KR mutation, we isolated lower LGP2 expressing clones (Fig EV3B and C). Even in the lower expressing LGP2 clones, the 4KR mutation enhanced the expression of IFN- $\beta$  and IP10 mRNA at later time points (Fig 5K and L). These data suggest that ubiquitinated LGP2 has a negative role in type I IFN expression only at late time points.

To further assess the role of LGP2 ubiquitination, we performed a microarray analysis of LGP2 and LGP2-4KR stably expressing cells (Fig 6A). Interestingly, there were many up- and down-regulated genes in LGP2-4KR expressing cells compared with WT LGP2 expressing cells after poly I:C stimulation (Fig EV4A), and several antiviral proteins were markedly down-regulated (Fig 6A). To validate this data, we used RT-qPCR, and found that short poly I:C-induced expression of SP100, ANKRD1, and PML mRNA was reduced by LGP2-4KR compared with wild-type LGP2 (Fig 6B and C). Previous studies have reported the antiviral activities of SP100, ANKRD1, and PML (Chelbi-Alix et al, 1998; Negorev et al, 2006; Bin et al, 2018). The LGP2-4KR mutant failed to upregulate the expression of PML and SP100 following influenza A virus infection in A549 cells (Fig 6D and E). The antiviral effects of PML bodies against influenza A virus infection have been previously reported (Gongora et al, 1997; Nguyen et al, 2001). Additionally, the expression levels of TLR5 and INPP5J induced by flu infection were reduced by the LGP2-4KR mutation compared with wild-type LGP2 (Fig 6F and G). TLR5 is a pattern recognition receptor for bacterial flagellin protein (Hayashi et al, 2001) and secondary bacterial

infection following primary influenza A virus infection is known to be serious in influenza patients (Morens et al, 2008). The SP100 and PML expression was reduced by MAVS knockout (Fig EV4B and C), thus the expression of the genes depends on MAVS. We found that phosphorylation of IRF3 essential for type I IFN expression was not impaired in LGP2 KO or LGP2-4KR mutant cells (Fig 6H and I). These data suggest that ubiquitination of LGP2 regulates the expression of antiviral genes in a RIG-I and MAVS-dependent manner but in an IRF3- and type I IFN-independent manner. It is notable that peroxisomal MAVS increases the expression of interferon stimulatory genes in a type I IFN-independent manner (Dixit et al, 2010). When we compared the localization of PLA signals of LGP2 and MAVS with that of peroxisome, we found that the 4KR mutation reduced the colocalization of the PLA signals with peroxisome (Fig 6J and K), implying that ubiquitination of LGP2 promotes localization of LGP2 on peroxisome.

Since Riplet mediated ubiquitination of LGP2, we investigated whether Riplet KO would exhibit a similar phenotype to the LGP2-4KR mutant. As expected, Riplet knockout cells failed to upregulate the expression of SP100 and PML mRNAs after short poly I:C stimulation at a late phase (Fig 7A). We found that knockout of LGP2 reduced the expression of SP100 and ANKRD1 induced by short poly I:C stimulation (Fig 7B), suggesting that non-ubiquitinated form of LGP2 plays a role in the expression of SP100 and ANKRD1. SP100 and ANKRD1 expression in resting cells were also reduced by MAVS or LGP2 KO by unknown mechanism (Figs 7B, and EV4B and D), but a previous study has reported LGP2 function in non-infected cells (Suthar et al, 2012).

Riplet knockout markedly reduced the SP100 expression induced by short poly I:C stimulation in A549 and mouse embryonic

**Figure 5. Ubiquitination of LGP2 attenuates type I IFN expression.**

- A RIG-I, WT LGP2, and KR mutants of LGP2 were transfected into HEK293 cells together with p125luc reporter plasmids. Luciferase activities were determined 24 h after transfection. The data represent the mean  $\pm$  SD ( $n = 3$ , t-test,  $*P < 0.05$ ). WCEs were subjected to SDS–PAGE, and the proteins were detected by western blotting (lower panels).
- B HEK293 cells stably expressing GFP (control), LGP2, or LGP2-4KR were transfected with p125luc reporter plasmids and then stimulated with indicated amounts of short poly I:C. WCEs were prepared 24 h after transfection and stimulation, and luciferase activity was determined. The proteins were subjected to SDS–PAGE and detected by western blotting with the indicated Abs. The data represent the mean  $\pm$  SD ( $n = 3$ , two-way ANOVA,  $*P < 0.05$ ).
- C–J HEK293 cells stably expressing GFP, LGP2, or LGP2-4KR were transfected with 200 ng/ml of short poly I:C (C–E), infected with SeV at MOI = 5 (F–H), or infected with influenza A virus (Flu) at MOI = 10 (I, J). Total RNA was isolated at the indicated time points. The expression of IFN- $\beta$ , IP-10, and Ccl5 mRNA was determined by RT-qPCR and normalized to GAPDH. The data represent the mean  $\pm$  SD ( $n = 3$ , two-way ANOVA,  $*P < 0.05$ ).
- K, L HEK293 cell clones stably expressing LGP2 or LGP2-4KR at lower levels (Fig EV5A) were transfected with short poly I:C, and the expression of mRNAs were determined by RT-qPCR. The data represent the mean  $\pm$  SD ( $n = 3$ , two-way ANOVA,  $*P < 0.05$ ).

Data information: All data are representative of at least two independent experiments, and “ $n$ ” represents the number of samples (biological replicates). Error bars represent standard deviation from the mean.

Source data are available online for this figure.



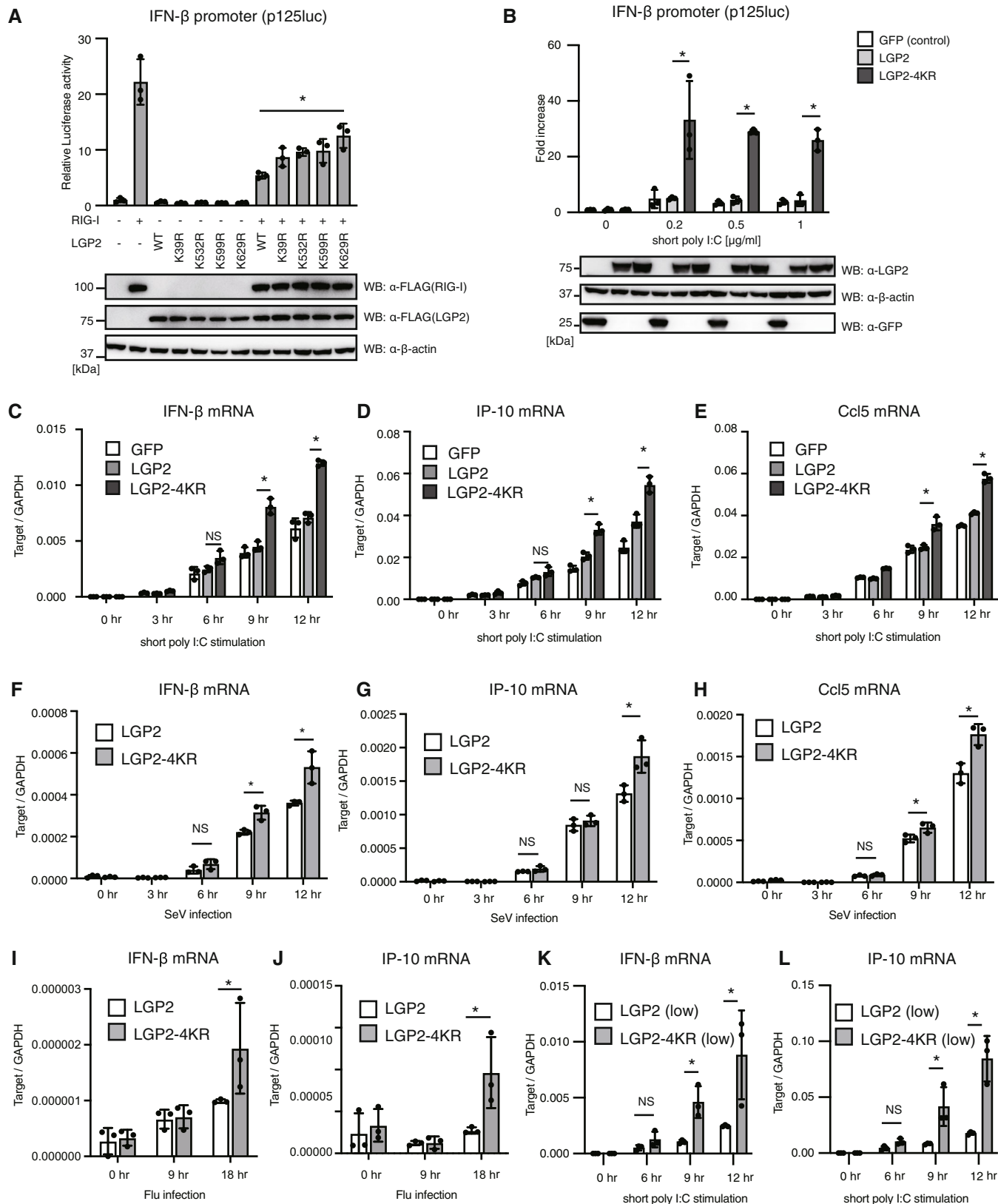


Figure 5.

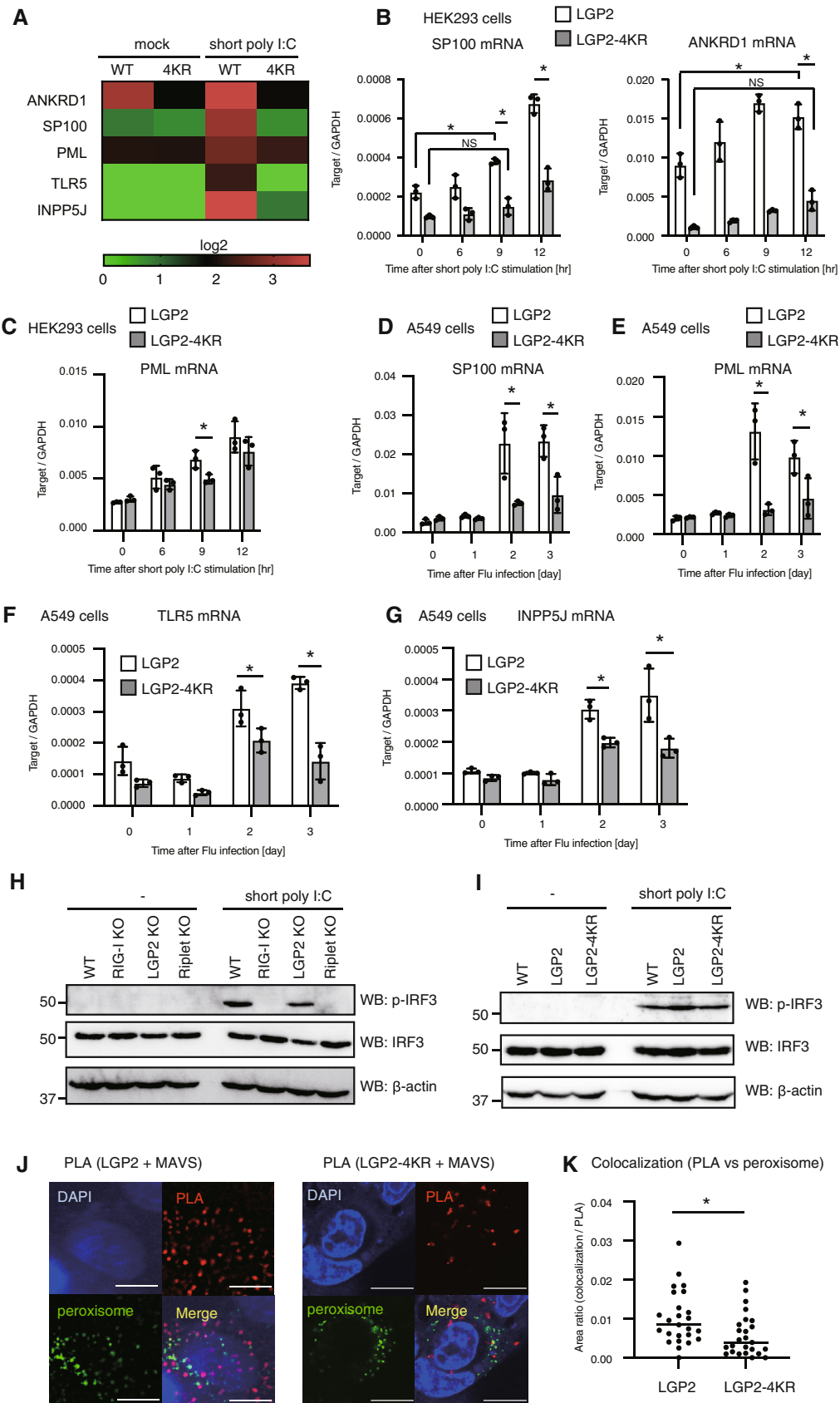


Figure 6.

**Figure 6. Ubiquitination of LGP2 increases the expression of antiviral genes.**

- A Microarray analysis was performed as described in [Materials and Methods](#). A heatmap of the microarray data of LGP2 and LGP2-4KR stably expressing cells stimulated with short poly I:C for 12 h.
- B, C LGP2 and LGP2-4KR stably expressing HEK293 cells were stimulated with 200 ng/ml of short poly I:C, and the expression of the genes at the indicated time points were determined by RT-qPCR and normalized to GAPDH ( $n = 3$ , two-way ANOVA,  $*P < 0.05$ ).
- D–G LGP2 and LGP2-4KR stably expressing A549 cells were infected with influenza A virus (Flu) at MOI = 10, and the expression of the genes at the indicated time points were determined by RT-qPCR and normalized to GAPDH ( $n = 3$ , two-way ANOVA,  $*P < 0.05$ ).
- H, I WT and indicated mutant HEK293 cells were stimulated with 200 ng/ml of short poly I:C for 8 h. WCEs were prepared and subjected to SDS-PAGE. The proteins were detected with indicated antibodies.
- J, K LGP2 and LGP2-4KR expressing vectors were transfected into HeLa cells with Riplet expressing vector. Eighteen hours after transfection, cells were fixed, and then the PLA signals of LGP2 and endogenous MAVS were detected. Peroxisome was visualized using CellLight Peroxisome-GFP reagent. Colocalization of GFP (peroxisome) and the PLA signals (red) were observed by confocal microscopy. Scale bars represent 10  $\mu\text{m}$  (J). The colocalization area was normalized to the area of the PLA signals ( $n = 25$ ,  $t$ -test,  $*P < 0.05$ ) (K).

Data information: All data except panel (A) are representative of at least two independent experiments, and “ $n$ ” represents the number of samples (biological replicates). Error bars represent standard deviation from the mean.

Source data are available online for this figure.

fibroblast cells (MEFs; Fig 7C and D). Moreover, knockout of Riplet reduced the expression of SP100 and PML mRNA in primary bone-marrow derived macrophages (BMMs) after influenza A virus infection at a late phase (Fig 7E). Furthermore, the PML protein level was reduced by knockout of Riplet in A549 cells infected with influenza A virus (Fig 7F). These data are consistent with our model that Riplet-mediated ubiquitination regulates the LGP2 function. However, it is still possible that the mutations on Riplet and/or LGP2 genes reduced RIG-I ubiquitination at a late phase, resulting in attenuated expression of the SP100 and PML mRNAs.

To further test whether the phenotype of LGP2-4KR depends on Riplet, we generated LGP2 or LGP2-4KR stably expressing HEK293 cells in Riplet KO background. If polyubiquitination of LGP2 by Riplet is responsible for LGP2-4KR phenotype, it is expected that the effect of LGP2-4KR mutation is canceled by Riplet KO. Since SP100 expression was hardly induced in Riplet KO HEK293 cells (Fig 7B), we compared the expression of IFN- $\beta$  mRNA in Riplet KO cells. As expected, LGP2-4KR mutations failed to increase IFN- $\beta$  mRNA expression during SeV infection in Riplet KO cells (Fig 7G), although LGP2-4KR mutation enhanced the expression in WT background (Figs 5C and 7G). Moreover, residual IFN- $\beta$  mRNA expression in response to short poly I:C in Riplet KO cells was not enhanced by LGP2-4KR mutation in Riplet KO background (Fig 7H). These double-mutant analyses also support our conclusion that Riplet-mediated ubiquitination of LGP2 regulates the expression of antiviral genes. Encephalomyocarditis virus (EMCV) is mainly recognized by MDA5, and we found that the LGP2-4KR mutation did not affect EMCV-induced IFN- $\beta$  mRNA expression (Fig 8A). This data suggests that polyubiquitination of LGP2 is not involved in MDA5-dependent pathway.

## Discussion

In this study, we found that that LGP2 undergoes K63-linked polyubiquitination. Polyubiquitination of LGP2 was delayed compared with RIG-I ubiquitination, and polyubiquitination of LGP2 affected its subcellular localization. Interestingly, K63-linked polyubiquitination attenuated type I IFN expression, whereas it increased the expression of antiviral genes including PML and SP100. Considering that excessive production of type I IFN is harmful to the host, we hypothesize that LGP2 is ubiquitinated to attenuate excessive type I

IFN expression without loss of the antiviral state of host cells at a late phase of viral infection (Fig EV5).

Previous studies have shown that Riplet induces RIG-I-dependent type I IFN expression (Oshiumi *et al*, 2010; Cadena *et al*, 2019). This study elucidated another aspect of Riplet. Our data showed that Riplet ubiquitinates LGP2 at a late phase. It is possible that the binding affinity of Riplet to RIG-I might be stronger than that to LGP2. Further biochemical analyses are required to reveal the mechanism underlying different ubiquitination kinetics.

Riplet is essential for RIG-I activation, but it is not involved in the MDA5-dependent pathway. MDA5 and RIG-I plays different roles in the recognition of viral RNAs. MDA5 prefers long dsRNAs compared to RIG-I, and EMCV is recognized by MDA5 but not RIG-I (Kato *et al*, 2006). Our data showed that the LGP2-4KR mutation did not affect type I IFN expression in response to EMCV infection. This suggests that Riplet-mediated ubiquitination of LGP2 does not affect MDA5 signaling. There are two possibilities. One possibility is that polyubiquitinated LGP2 does not affect MDA5 function, and the other is that LGP2 is ubiquitinated by Riplet only when RIG-I is activated. Considering that Riplet is a coreceptor of RIG-I (Cadena *et al*, 2019), we prefer the second model that LGP2 is ubiquitinated when RIG-I is activated. Further studies are required to test these hypotheses.

RIG-I induces two major signaling pathways: the mitochondrial MAVS-dependent pathway and the peroxisomal MAVS-dependent pathway (Dixit *et al*, 2010). Although ISG expression is controlled by type I IFN, peroxisomal MAVS directly induces the expression of ISGs (Dixit *et al*, 2010). We found that a part of the PLA signals of LGP2 and MAVS colocalized with peroxisome, and that the colocalization was reduced by the 4KR mutation. This data implies that ubiquitination of LGP2 promotes the localization of the protein on peroxisome, in which MAVS can induce the ISGs expression in a type I IFN independent manner. In contrast, the 4KR mutation or LGP2 KO hardly affected the IRF3 activation by RIG-I. Considering that IFN- $\beta$  promoter activities were regulated not only by IRF3 but also NF- $\kappa$ B, and AP-1 transcription factors (Honda *et al*, 2006), it is possible that LGP2 ubiquitination attenuated the activation of NF- $\kappa$ B, AP-1, and/or other factors to reduce type I IFN expression and to increase ISGs expression. Further studies are required to reveal whether LGP2 ubiquitination activates peroxisomal but not mitochondrial MAVS.

Mass spectrometry analysis revealed four ubiquitination sites in LGP2. This analysis suggests the covalent binding of ubiquitin to

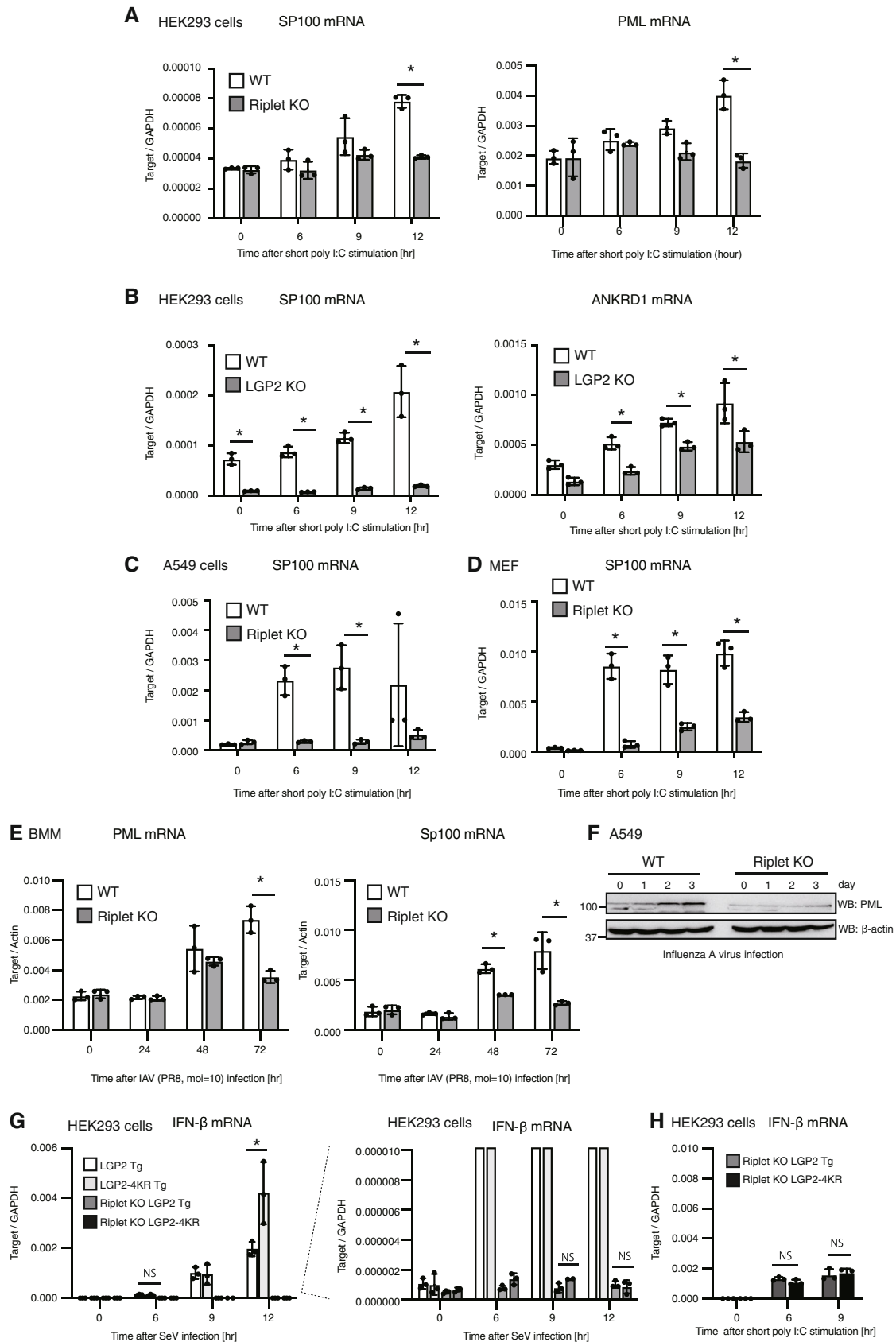
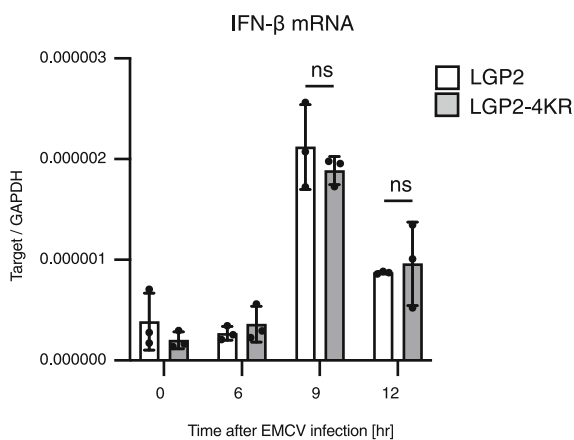


Figure 7.

**Figure 7. Riplet is required for the antiviral gene expression at a late phase.**

- A, B WT, LGP2 KO, and Riplet KO HEK293 cells were stimulated with 200 ng/ml of short poly I:C. The expression of SP100, PML, and ANKRD1 mRNA was determined by RT-qPCR and normalized to GAPDH ( $n = 3$ , two-way ANOVA,  $*P < 0.05$ ).
- C, D WT and Riplet KO A549 (C) and MEF (D) cells were stimulated with 200 ng/ml of short poly I:C. The expression of SP100 was determined by RT-qPCR ( $n = 3$ , two-way ANOVA,  $*P < 0.05$ ).
- E WT and Riplet KO BMM were infected with influenza A virus (Flu) at MOI = 10. PML and SP100 mRNA expression was determined by RT-qPCR ( $n = 3$ , two-way ANOVA,  $*P < 0.05$ ).
- F WT and Riplet KO A549 cells were infected with influenza A virus infection at MOI = 10. WCE was prepared at the indicated time points and subjected to SDS-PAGE. Proteins were detected by western blotting with the indicated antibody.
- G, H LGP2 or LGP2-4KR stably expressing WT or Riplet KO HEK293 cells were infected with SeV (G) or stimulated with 200 ng/ml of short poly I:C (H). IFN- $\beta$  mRNA levels at indicated time points were determined by RT-qPCR. ( $n = 3$ , two-way ANOVA,  $*P < 0.05$ , ns, not significant ( $P > 0.05$ )). Right graph in panel (G) is an enlargement of Y-axis of the left graph (dotted line).

Data information: All data are representative of at least two independent experiments, and “n” represents the number of samples (biological replicates). Error bars represent standard deviation from the mean.  
Source data are available online for this figure.

**Figure 8. Type I IFN expression in LGP2 mutants after EMCV infection.**

LGP2 or LGP2-4KR stably expressing HEK293 cells were infected with EMCV at MOI = 20, and RNA was extracted at indicated time points. IFN- $\beta$  mRNA levels were determined by RT-qPCR ( $n = 3$ , two-way ANOVA, ns, not significant ( $P > 0.05$ )). The data are representative of two independent experiments. “n” represents the number of samples (biological replicates). Error bars represent standard deviation from the mean.

the four K residues of the LGP2 protein. However, residual ubiquitination was still detected in LGP2 KR mutant protein. Thus, we cannot exclude the possibility that polyubiquitination at other sites on LGP2 would exhibit different effects on antiviral gene expression. Since the diglycine motif on peptide detected by mass spectrometry is also observed in other modifications, such as ISGylation, it is still possible that the K residues harbored ISGylation and/or other modifications as well as ubiquitination. Proteins are phosphorylated at multiple sites and phosphorylation at different sites may exhibit opposing effects on the protein function. Hur and colleagues previously have reported that TRIM14 binds to LGP2 *in vitro* (Kato *et al*, 2021). Since TRIM14 is a member of TRIM family that includes ubiquitin ligases, TRIM14-mediated polyubiquitination of LGP2 might exhibit a different effect on LGP2 function.

First, LGP2 is reported to be a negative regulator of RIG-I signaling (Yoneyama *et al*, 2005). Several studies reported a negative role of LGP2 in the antiviral innate immune response (Saito *et al*, 2007; Venkataraman *et al*, 2007; Si-Tahar *et al*, 2014). Conversely, Akira

and colleagues reported a positive role for LGP2 in RIG-I signaling (Satoh *et al*, 2010). The mechanisms underlying these apparent discrepancies were unclear. In the present study, we found that LGP2 has both positive and negative roles in RIG-I-mediated type I IFN expression. We prefer the interpretation that non-ubiquitinated LGP2 promotes RIG-I-dependent type I IFN expression, however, polyubiquitinated LGP2 attenuates the type I IFN expression. This model could explain the reason why there are several contradictory reports. Some experimental conditions may affect the ubiquitination status of endogenous LGP2, which results in a different phenotype depending on the cells or experimental conditions.

Many viruses have evolved to escape the host innate immune response (Chan & Gack, 2016; Chiang *et al*, 2021). Indeed, recent studies have elucidated the immunosuppressive effects of viral proteins of SARS-CoV-2 that recently caused a global pandemic (Kouwaki *et al*, 2021; Liu *et al*, 2021; Wu *et al*, 2021). Thus, we expect that the molecular mechanisms elucidated in this study will be useful for understanding the pathogenesis of viral infection.

RLRs are also involved in anti-tumor immune responses. It is notable that LGP2 regulates CD4<sup>+</sup> or CD8<sup>+</sup> T cells (Chopy *et al*, 2011; Leavy, 2012; Suthar *et al*, 2012; Zheng *et al*, 2020). LGP2 promotes the survival of antigen-specific CD8<sup>+</sup> T cells (Suthar *et al*, 2012), and is involved in anti-tumor immune responses (Zheng *et al*, 2020). Recently, we found that knockout of Riplet enhanced anti-tumor immune responses of CD8<sup>+</sup> T cells induced by stimulated dendritic cells or anti-PD-L1 antibody (Iwamoto *et al*, 2022). Considering that Riplet regulated LGP2 function via ubiquitination, it is possible that LGP2 of CD8<sup>+</sup> T cells might enhance the efficacy of anti-PD1 or anti-PDL1 anti-cancer therapy. Further studies will elucidate a crucial role of LGP2 ubiquitination in anti-cancer immune therapy.

## Materials and Methods

### Cell lines

Riplet, MAVS, and LGP2 KO cells were generated using a CRISPR/Cas9 system. The guide sequence (See Appendix Table S1) was cloned into the BbsI restriction site of a pX459 plasmid carrying Cas9 and puromycin resistance genes. The plasmids carrying the guide sequence were transfected into HEK293, A549, and HeLa cells.

After 36 h of transfection, the cells were treated with 1 µg/ml of puromycin for 3 days, and then were cultured in fresh medium without puromycin for 2 days. Finally, cells were seeded into 96-well plates and cultured for 7–10 days to obtain a single clone, which was transferred into 24-well plates. Western blot analysis was performed to confirm KO of the target gene.

### Constructs

cDNAs encoding the full-length ORFs of LGP2 were amplified with a cDNA library from HEK293 cells, and were cloned into the *KpnI* restriction site of pEF-BOS using an In-Fusion Cloning Kit (TaKaRa Bio.). A FLAG-tag sequence was inserted just after the start codon. The KR mutations were introduced into the LGP2 gene on the expression plasmid using overlapping forward and reverse primers. Full-length LGP2 KR mutants were amplified using two fragments as templates and cloned into the pEF-BOS-FLAG vector.

### Cells and viruses

HEK293 cells were maintained in DMEM (low Glc) supplemented with 10% heat-inactivated FCS and penicillin–streptomycin solution. HEK293FT and A549 cells were incubated in DMEM (high Glc) supplemented with 10% heat-inactivated FCS and penicillin–streptomycin solution. HeLa cells were cultured in MEM supplemented with 10% heat-inactivated FCS and penicillin–streptomycin solution. The cells were grown in a humidified incubator with an atmosphere of 5% CO<sub>2</sub>. Riplet KO mice, described previously (Oshiumi *et al*, 2010), were back-crossed over five times with wild-type C57BL6 mice. Mouse embryonic fibroblasts were prepared from day 12.5–13.5 embryos. Bone-marrow-derived cells were prepared from the femur and tibia, and cultured with RPMI1640 containing 10% FCS, 100 µM 2-Me, and 10 ng/ml of M-CSF for 1 week to obtain BMMs. LGP2 KO and Riplet KO HEK293 cells were generated by CRISPR-Cas9 systems. Knockout of each gene was confirmed by sequencing genome region targeted by CRISPR-Cas9. SeV was amplified using chicken egg, and the number of plaque-forming units was determined by a plaque assay. The cells were infected with SeV at MOI = 5 to determine cytokine expression after SeV infection. Influenza A virus (PR8 strain; Flu) was amplified using chicken egg and the plaque-forming units were determined by a plaque assay using MDCK cells. EMCV was purchased from ATCC (VR-1762), and were amplified using Vero cells. EMCV viral titers were determined by plaque assay with Vero cells. All mice were maintained at the Center for Animal Resources and Development of Kumamoto University (Kumamoto, Japan) in a specific pathogen-free environment. All animal experimental procedures were approved by the Institutional Animal Committee of Kumamoto University (A2019-088) and performed in accordance with the guidelines.

### Western blot analysis

Cells were washed with PBS and lysed in NP-40 lysis buffer [20 mM Tris–HCl (pH 7.5), 125 mM NaCl, 1 mM EDTA, 10% Glycerol, 1% NP-40, 30 mM NaF, and 5 mM Na<sub>3</sub>VO<sub>4</sub>] in the presence of complete protease inhibitor cocktail (Roche). The cell lysates were incubated on ice for 30 min and were then centrifuged for 20 min at 20,400 g

at 4°C. The supernatants were transferred to 1.5 ml tubes and suspended in 2 × Laemmli sample buffer containing β-mercaptoethanol. The cell lysates were boiled for 5 min at 95°C. All samples and protein markers (Bio-Rad) were each loaded into separate wells for SDS–PAGE in a Tris-glycine-SDS running buffer and then transferred to PVDF membranes. The membranes were blocked with 5% skim milk in rinse buffer [0.1% Tween 20, 10 mM Tris–HCl (pH 7.5), 0.8% NaCl, and 1 mM EDTA], and was incubated with 1st Ab (1:1,000) at 4°C overnight, and then incubated with HRP-conjugated secondary Ab (1:10,000) for 60 min at room temperature. The immunoblots were visualized with ECL Prime Western Blotting Detection Reagent (GE Healthcare) and detected using the ChemiDoc Touch Imaging System (Bio-Rad). Anti-RIG-I antibody (Alme-1; Cat# AG-20B-009), anti-LGP2 antibody (Cat# 12869), anti-β-actin antibody (Cat# AMAb91241) were purchased from AdipoGen, Cell Signaling Technology (CST), and Sigma-Aldrich, respectively. Anti-Rabbit IgG, HRP-Linked whole Ab Donkey (Cat# NA934), and anti-mouse IgG HRP-linked whole Ab sheep (Cat#931) were purchased from GE Healthcare. Anti-K63-specific ubiquitin mouse (Cat#05-1313) and rabbit antibodies (Cat#05-1308) were purchased from Millipore. Anti-HA antibody (Cat#H6908) and anti-FLAG-antibody (Cat#F3165) were purchased from Sigma-Aldrich, and anti-c-Myc antibody (Cat#626802) were purchased from BioLegend.

### Immunoprecipitation

HEK293FT (5 × 10<sup>5</sup>) cells were cultured in a 6-well plate for overnight and then transfected with expression vectors using Lipofectamine 2000. The total amount of plasmid was maintained at 1 µg by adding empty plasmid. The cells were harvested and washed with PBS after 24 h of transfection, and lysed with lysis buffer containing a protease inhibitor cocktail. The cell lysates were kept on ice for 30 min and then centrifuged at 20,400 g for 20 min at 4°C. The supernatants were transferred to 1.5 ml tubes. The lysates were pre-treated with protein G sepharose beads at 4°C for 60 min with rotation and then centrifuged to remove the beads. Anti-FLAG (1:150) Ab was added to the lysates and they were incubated for 2 h at 4°C with rotation. The washed protein G sepharose beads were added to the lysates containing the Ab, and incubated overnight with rotation. Then, the protein G sepharose beads were collected by centrifugation and washed three times with lysis buffer. The precipitated samples were analyzed by western blot analysis.

### PLA

HEK293 and A549 cells were seeded on a glass-bottom plate and fixed with 4% PFA for 15 min at room temperature and permeabilized with 0.3% Triton-X100 in PBS for 60 min at room temperature. Subsequently, PLA signals were detected by a Duolink In Situ PLA Kit (Sigma-Aldrich) according to the manufacturer's instructions. Briefly, the cells were blocked with blocking buffer, labeled with primary Ab, and incubated with ligation solution to hybridize the positive and negative probes. The cells were then incubated with green or red PLA detection reagent to initiate DNA synthesis with dye-conjugated nucleotides. The indicated number of cells were randomly chosen and observed by confocal microscopy (FV1200; Olympus) to determine the percentage of PLA-positive cells and the

number of PLA signals in the cell. Rhodamin-conjugated short poly I:C (LMW; tlr1-piwr) were purchased from InvivoGen. To observe peroxisome, 20  $\mu$ l of CellLight Peroxisome-GFP reagents (ThermoFisher Scientific) were added into the cells in a 24-well plate before cells were transfected with FLAG-LGP2 or FLAG-LGP2-4KR expressing vectors. To compare the colocalization of the PLA signals and peroxisome, 20 places, in which dozens of cells were included, were randomly selected. The colocalization area ratio was calculated by dividing the colocalization area with the PLA signal area in each place.

### Reporter gene assay

We seeded  $1 \times 10^5$  of HEK293 cells into 24-well plates in triplicate and transfected the cells with an expression vector together with the p-125 Luc reporter (100 ng/well) and phRL-TK (10 ng/well, Promega) plasmids. The phRL-TK (HSV-thymidine kinase promoter) plasmid encodes *Renilla* luciferase and was used as an internal control. An empty plasmid was added to ensure that each transfection received the same amount of total DNA. After 24 h of transfection, luciferase assays were performed using a Dual Luciferase Assay Kit (Promega). Luciferase activity was normalized to that of *Renilla* luciferase.

### Quantitative real-time PCR

We seeded  $1 \times 10^5$  of HEK293 cells into 24-well plates. The cells were then transfected with 100 ng of short poly I:C using Lipofectamine 2000 to determine cytokine expression after stimulation. Total RNA was isolated from the cells using TRIzol reagent (Invitrogen) according to the manufacturer's instructions. cDNA was generated from the total RNA using a High-Capacity cDNA Reverse Transcription Kit (Applied Biosystems). The target mRNA was quantified with Power SYBR Green Master Mix (Applied Biosystems) using the ViiA-7 Real-Time PCR system (Applied Biosystems), and the expression levels were normalized to GAPDH. Short poly I:C (LMW poly I:C) were purchased from InvivoGen (tlrl-picw).

### Lentivirus production

HEK293FT cells ( $2 \times 10^6$ ) were seeded onto a 10 cm dish and incubated at 37°C for 1 day. GFP, LGP2, and LGP2 4KR ORFs were cloned into the FU1PW lentiviral vector and co-transfected with packaging plasmids into HEK293FT cells. After 3 days of transfection, the viruses were harvested and filtered (0.22  $\mu$ m filter, Millipore) and used to infect HEK293 or Riplet KO HEK293 cells in the presence of polybrene (10  $\mu$ g/ml). The infected cells were selected with the application of puromycin (1  $\mu$ g/ml) for 3 days.

### Nano-liquid chromatography–tandem mass spectrometry (LC–MS/MS)

FLAG-tagged LGP2 and Riplet expression vectors were transfected into HEK293 cells. After 24 h, cell lysates were prepared, and LGP2 was purified using anti-FLAG monoclonal Abs. The isolated LGP2 was subjected to SDS–PAGE and stained with CBB. LGP2 bands were excised from the gel. Then, the proteins in each gel slice were

subjected to reduction with 10 mM dithiothreitol (DDT), at 56°C for 1 h, alkylation with 55 mM iodoacetamide at room temperature for 45 min in the dark, and digestion with 10  $\mu$ g/ml modified trypsin (Promega) at 37°C for 16 h. The resulting peptides were extracted with 1% trifluoroacetic acid and 50% acetonitrile, dried under a vacuum, and dissolved in 2% acetonitrile and 0.1% formic acid. The peptides were then fractionated by C18 reverse-phase chromatography (Advance Nanoflow UHPLC System; AMR Inc.) and applied directly into a hybrid linear ion trap mass spectrometer (LTQ Orbitrap Velos Pro; Thermo Fisher Scientific) with Advanced Captive Spray SOURCE (AMR Inc.) as the ion source. The mass spectrometer was programmed to perform 11 successive scans, with the first consisting of a full MS scan from 350–1,800 m/z by FT-ICR at a resolution of 60,000. Scans 2–11 were of data-dependent scans of the top 10 abundant ions obtained in the first scan, by ion trap. Automatic MS/MS spectra were obtained from the highest peak in each scan by setting the relative collision energy to 35% and the exclusion time to 20 s for molecules in the same m/z value range. The molecular masses of the resulting peptides were searched against the Uniprot Proteome Homo sapiens database (downloaded 2018.12.13) using the Mascot v2.6 program via Proteome Discoverer v2.2 (Thermo Fisher Scientific) with the false discovery rate (FDR) set at 0.01. Cysteine carbamidomethylation was set as a fixed modification. The oxidation of methionine, acetylation of protein N-termini, and ubiquitination of lysine were set as variable modifications. The number of missed cleavage sites was set as 2. Obtained LC–MS/MS data was analyzed with Proteome Discoverer 2.2 (PD2.2) software framework (Thermo Scientific) to quantify ubiquitination of LGP2 proteins in WT and Riplet overexpressing cells.

### Microarray

LGP2 and LGP2-4KR HEK293 cells ( $1 \times 10^5$ ) were cultured in 24-well plates and were transfected with 100 ng/ml of short poly I:C for 12 h. Total RNA was isolated using TRIzol reagent, and three independent samples were mixed to normalize the differences among each well. cDNA and Amino Allyl aRNA were synthesized using the Amino Allyl MessageAmp II aRNA amplification kit (Ambion#1753). Cy5Dye Coupling and fragmentation were performed using the protocol supplied by TORAY. Hybridization was performed for 16 h at 37°C on a rotary shaker (250 rpm). Hybridization buffer and washing protocol was done using the protocol supplied by TORAY. A 3D-Gene Scanner (TORAY) was used for scanning. Images were quantified using Extraction (TORAY). The raw data for each spot was normalized by substitution with a mean intensity of the background signal determined by all blank spot signaling intensities of 95% confidence intervals. The assigned GEO accession number is GSE176363.

### Quantification and statistical analysis

All qPCR assays and reporter gene assays were performed using three independent samples (biological replicates;  $n = 3$ ). Error bars represent the standard deviation (SD). Statistical significance ( $P$ -value) was determined using a two-tailed Student's  $t$ -test, one-way ANOVA, or two-way ANOVA using Prism v7.0a (GraphPad Software) and MS-Excel (Microsoft Corp) software. \* $P < 0.05$ .

## Data availability

Microarray data have been deposited in Gene Expression Omnibus (GEO accession number: GSE176363; <https://www.ncbi.nlm.nih.gov/geo/query/acc.cgi?acc=GSE176363>).

**Expanded View** for this article is available [online](#).

## Acknowledgements

We thank our laboratory members for helpful discussions and two researchers for helpful comments on our manuscript. This work was supported in part by Grants-in-Aid from Japan Society for the Promotion of Science (JSPS) (21K07069) and KOSE Cosmetology Research Foundation.

## Author contributions

**Takahisa Kouwaki:** Investigation; writing – review and editing.

**Tasuku Nishimura:** Investigation. **Guanming Wang:** Investigation.

**Reiko Nakagawa:** Investigation. **Hiroyuki Oshiumi:** Supervision; writing – original draft; writing – review and editing.

## Disclosure and competing interests statement

The authors declare that they have no conflict of interest.

## References

- Bin L, Li X, Richers B, Streib JE, Hu JW, Taylor P, Leung DYM (2018) Ankyrin repeat domain 1 regulates innate immune responses against herpes simplex virus 1: a potential role in eczema herpeticum. *J Allergy Clin Immunol* 141: 2085–2093
- Cadena C, Ahmad S, Xavier A, Willemsen J, Park S, Park JW, Oh SW, Fujita T, Hou F, Binder M *et al* (2019) Ubiquitin-dependent and -independent roles of E3 ligase RIPLET in innate immunity. *Cell* 177: 1187–1200
- Chan YK, Gack MU (2016) Viral evasion of intracellular DNA and RNA sensing. *Nat Rev Microbiol* 14: 360–373
- Chelbi-Alix MK, Quignon F, Pelicano L, Koken MH, de The H (1998) Resistance to virus infection conferred by the interferon-induced promyelocytic leukemia protein. *J Virol* 72: 1043–1051
- Chiang C, Gack MU (2017) Post-translational control of intracellular pathogen sensing pathways. *Trends Immunol* 38: 39–52
- Chiang C, Liu G, Gack MU (2021) Viral evasion of RIG-I-like receptor-mediated immunity through dysregulation of ubiquitination and ISGylation. *Viruses* 13: 182
- Chopy D, Pothlichet J, Lafage M, Megret F, Fiette L, Si-Tahar M, Lafon M (2011) Ambivalent role of the innate immune response in rabies virus pathogenesis. *J Virol* 85: 6657–6668
- Cui S, Eisenacher K, Kirchofer A, Brzozka K, Lammens A, Lammens K, Fujita T, Conzelmann KK, Krug A, Hopfner KP (2008) The C-terminal regulatory domain is the RNA 5'-triphosphate sensor of RIG-I. *Mol Cell* 29: 169–179
- Davis ME, Gack MU (2015) Ubiquitination in the antiviral immune response. *Virology* 479–480: 52–65
- Dixit E, Boulant S, Zhang Y, Lee AS, Odendall C, Shum B, Hacohen N, Chen ZJ, Whelan SP, Franssen M *et al* (2010) Peroxisomes are signaling platforms for antiviral innate immunity. *Cell* 141: 668–681
- Fredriksson S, Gullberg M, Jarvius J, Olsson C, Pietras K, Gustafsdottir SM, Ostman A, Landegren U (2002) Protein detection using proximity-dependent DNA ligation assays. *Nat Biotechnol* 20: 473–477
- Gack MU, Shin YC, Joo CH, Urano T, Liang C, Sun L, Takeuchi O, Akira S, Chen Z, Inoue S *et al* (2007) TRIM25 RING-finger E3 ubiquitin ligase is essential for RIG-I-mediated antiviral activity. *Nature* 446: 916–920
- Gongora C, David G, Pintard L, Tissot C, Hua TD, Dejean A, Mechti N (1997) Molecular cloning of a new interferon-induced PML nuclear body-associated protein. *J Biol Chem* 272: 19457–19463
- Hayashi F, Smith KD, Ozinsky A, Hawn TR, Yi EC, Goodlett DR, Eng JK, Akira S, Underhill DM, Aderem A (2001) The innate immune response to bacterial flagellin is mediated by toll-like receptor 5. *Nature* 410: 1099–1103
- Honda K, Takaoka A, Taniguchi T (2006) Type I interferon [corrected] gene induction by the interferon regulatory factor family of transcription factors. *Immunity* 25: 349–360
- Hur S (2019) Double-stranded RNA sensors and modulators in innate immunity. *Annu Rev Immunol* 37: 349–375
- Iwamoto A, Tsukamoto H, Nakayama H, Oshiumi H (2022) E3 ubiquitin ligase Riplet is expressed in T cells and suppresses T cell-mediated antitumor immune responses. *J Immunol* 208: 2067–2076
- Jang MA, Kim EK, Now H, Nguyen NT, Kim WJ, Yoo JY, Lee J, Jeong YM, Kim CH, Kim OH *et al* (2015) Mutations in DDX58, which encodes RIG-I, cause atypical singleton-Merten syndrome. *Am J Hum Genet* 96: 266–274
- Kato H, Takeuchi O, Sato S, Yoneyama M, Yamamoto M, Matsui K, Uematsu S, Jung A, Kawai T, Ishii KJ *et al* (2006) Differential roles of MDA5 and RIG-I helicases in the recognition of RNA viruses. *Nature* 441: 101–105
- Kato H, Takeuchi O, Mikamo-Satoh E, Hirai R, Kawai T, Matsushita K, Hiiragi A, Dermody TS, Fujita T, Akira S (2008) Length-dependent recognition of double-stranded ribonucleic acids by retinoic acid-inducible gene-I and melanoma differentiation-associated gene 5. *J Exp Med* 205: 1601–1610
- Kato K, Ahmad S, Zhu Z, Young JM, Mu X, Park S, Malik HS, Hur S (2021) Structural analysis of RIG-I-like receptors reveals ancient rules of engagement between diverse RNA helicases and TRIM ubiquitin ligases. *Mol Cell* 81: 599–613
- Kawai T, Takahashi K, Sato S, Coban C, Kumar H, Kato H, Ishii KJ, Takeuchi O, Akira S (2005) IPS-1, an adaptor triggering RIG-I- and Mda5-mediated type I interferon induction. *Nat Immunol* 6: 981–988
- Kouwaki T, Nishimura T, Wang G, Oshiumi H (2021) RIG-I-like receptor-mediated recognition of viral genomic RNA of severe acute respiratory syndrome Coronavirus-2 and viral escape from the host innate immune responses. *Front Immunol* 12: 700926
- Kuniyoshi K, Takeuchi O, Pandey S, Satoh T, Iwasaki H, Akira S, Kawai T (2014) Pivotal role of RNA-binding E3 ubiquitin ligase MEX3C in RIG-I-mediated antiviral innate immunity. *Proc Natl Acad Sci USA* 111: 5646–5651
- Leavy O (2012) Antiviral immunity: LGP2 rigs CD8+ T cells for survival. *Nat Rev Immunol* 12: 616–617
- Liu G, Lee JH, Parker ZM, Acharya D, Chiang JJ, van Gent M, Riedl W, Davis-Gardner ME, Wies E, Chiang C *et al* (2021) ISG15-dependent activation of the sensor MDA5 is antagonized by the SARS-CoV-2 papain-like protease to evade host innate immunity. *Nat Microbiol* 6: 467–478
- Makela SM, Osterlund P, Westenius V, Latvala S, Diamond MS, Gale M Jr, Julkunen I (2015) RIG-I signaling is essential for influenza B virus-induced rapid interferon gene expression. *J Virol* 89: 12014–12025
- Meylan E, Curran J, Hofmann K, Moradpour D, Binder M, Bartenschlager R, Tschopp J (2005) Cardif is an adaptor protein in the RIG-I antiviral pathway and is targeted by hepatitis C virus. *Nature* 437: 1167–1172
- Morens DM, Taubenberger JK, Fauci AS (2008) Predominant role of bacterial pneumonia as a cause of death in pandemic influenza: implications for pandemic influenza preparedness. *J Infect Dis* 198: 962–970



- Negorev DG, Vladimirova OV, Ivanov A, Rauscher F III, Maul GG (2006) Differential role of Sp100 isoforms in interferon-mediated repression of herpes simplex virus type 1 immediate-early protein expression. *J Virol* 80: 8019–8029
- Nguyen LH, Espert L, Mechti N, Wilson DM III (2001) The human interferon- and estrogen-regulated ISG20/HEM45 gene product degrades single-stranded RNA and DNA in vitro. *Biochemistry* 40: 7174–7179
- Onomoto K, Onoguchi K, Yoneyama M (2021) Regulation of RIG-I-like receptor-mediated signaling: interaction between host and viral factors. *Cell Mol Immunol* 18: 539–555
- Oshiumi H, Matsumoto M, Hatakeyama S, Seya T (2009) Riplet/RNF135, a RING finger protein, ubiquitinates RIG-I to promote interferon-beta induction during the early phase of viral infection. *J Biol Chem* 284: 807–817
- Oshiumi H, Miyashita M, Inoue N, Okabe M, Matsumoto M, Seya T (2010) The ubiquitin ligase Riplet is essential for RIG-I-dependent innate immune responses to RNA virus infection. *Cell Host Microbe* 8: 496–509
- Oshiumi H, Miyashita M, Matsumoto M, Seya T (2013) A distinct role of Riplet-mediated K63-linked polyubiquitination of the RIG-I repressor domain in human antiviral innate immune responses. *PLoS Pathog* 9: e1003533
- Saito T, Hirai R, Loo YM, Owen D, Johnson CL, Sinha SC, Akira S, Fujita T, Gale M Jr (2007) Regulation of innate antiviral defenses through a shared repressor domain in RIG-I and LGP2. *Proc Natl Acad Sci USA* 104: 582–587
- Satoh T, Kato H, Kumagai Y, Yoneyama M, Sato S, Matsushita K, Tsujimura T, Fujita T, Akira S, Takeuchi O (2010) LGP2 is a positive regulator of RIG-I- and MDA5-mediated antiviral responses. *Proc Natl Acad Sci USA* 107: 1512–1517
- Seth RB, Sun L, Ea CK, Chen ZJ (2005) Identification and characterization of MAVS, a mitochondrial antiviral signaling protein that activates NF-kappaB and IRF 3. *Cell* 122: 669–682
- Si-Tahar M, Blanc F, Furio L, Choppy D, Balloy V, Lafon M, Chignard M, Fiette L, Langa F, Charneau P et al (2014) Protective role of LGP2 in influenza virus pathogenesis. *J Infect Dis* 210: 214–223
- Soderberg O, Gullberg M, Jarvius M, Ridderstrale K, Leuchowius KJ, Jarvius J, Wester K, Hydbring P, Bahram F, Larsson LG et al (2006) Direct observation of individual endogenous protein complexes in situ by proximity ligation. *Nat Methods* 3: 995–1000
- Suthar MS, Ramos HJ, Brassil MM, Netland J, Chappell CP, Blahnik G, McMillan A, Diamond MS, Clark EA, Bevan MJ et al (2012) The RIG-I-like receptor LGP2 controls CD8(+) T cell survival and fitness. *Immunity* 37: 235–248
- Venkataraman T, Valdes M, Elsby R, Kakuta S, Caceres G, Saijo S, Iwakura Y, Barber GN (2007) Loss of DExD/H box RNA helicase LGP2 manifests disparate antiviral responses. *J Immunol* 178: 6444–6455
- Wu J, Shi Y, Pan X, Wu S, Hou R, Zhang Y, Zhong T, Tang H, Du W, Wang L et al (2021) SARS-CoV-2 ORF9b inhibits RIG-I-MAVS antiviral signaling by interrupting K63-linked ubiquitination of NEMO. *Cell Rep* 34: 108761
- Xu LG, Wang YY, Han KJ, Li LY, Zhai Z, Shu HB (2005) VISA is an adapter protein required for virus-triggered IFN-beta signaling. *Mol Cell* 19: 727–740
- Yamada T, Sato S, Sotoyama Y, Orba Y, Sawa H, Yamauchi H, Sasaki M, Takaoka A (2021) RIG-I triggers a signaling-abortive anti-SARS-CoV-2 defense in human lung cells. *Nat Immunol* 22: 820–828
- Yan J, Li Q, Mao AP, Hu MM, Shu HB (2014) TRIM4 modulates type I interferon induction and cellular antiviral response by targeting RIG-I for K63-linked ubiquitination. *J Mol Cell Biol* 6: 154–163
- Yoneyama M, Kikuchi M, Matsumoto K, Imaizumi T, Miyagishi M, Taira K, Foy E, Loo YM, Gale M Jr, Akira S et al (2005) Shared and unique functions of the DExD/H-box helicases RIG-I, MDA5, and LGP2 in antiviral innate immunity. *J Immunol* 175: 2851–2858
- Zheng W, Ranoa DRE, Huang X, Hou Y, Yang K, Poli EC, Beckett MA, Fu YX, Weichselbaum RR (2020) RIG-I-like receptor LGP2 is required for tumor control by radiotherapy. *Cancer Res* 80: 5633–5641